Spin-triplet topological excitonic insulators in two-dimensional materials

Huaiyuan Yang [1], Jiaxi Zeng,[1] Yuelin Shao [2,3,*] Yuanfeng Xu,[4] Xi Dai,[5] and Xin-Zheng Li [1,6,7,†]

[1]*State Key Laboratory for Artificial Microstructure and Mesoscopic Physics, Frontier Science Center for Nano-optoelectronics and School of Physics, Peking University, Beijing 100871, People's Republic of China*

[2]*Beijing National Laboratory for Condensed Matter Physics and Institute of Physics, Chinese Academy of Sciences, Beijing 100190, People's Republic of China*

[3]*School of Physical Sciences, University of Chinese Academy of Sciences, Beijing 100049, People's Republic of China*

[4]*Center for Correlated Matter, School of Physics, Zhejiang University, No. 866, Yuhangtang Road, Xihu District, Zhejiang Province, Hangzhou 310058, People's Republic of China*

[5]*Department of Physics, Hong Kong University of Science and Technology, Clear Water Bay, Kowloon 999077, Hong Kong*

[6]*Interdisciplinary Institute of Light-Element Quantum Materials, Research Center for Light-Element Advanced Materials, and Collaborative Innovation Center of Quantum Matter, Peking University, Beijing 100871, People's Republic of China*

[7]*Peking University Yangtze Delta Institute of Optoelectronics, Nantong, Jiangsu 226010, People's Republic of China*

Quantum spin-Hall insulators (QSHIs) possess nontrivial band topology. Using first-principles many-body perturbation theory (GW+Bathe-Salpeter equation), we show that excitonic insulators (EIs) can exist in QSHIs AsO and $Mo_2TiC_2O_2$ with nonvanishing band gaps. Their single-particle topological properties can be described by the same low-energy model, and we show that the EI phase in this model is of spin-triplet type due to the nontrivial band geometry. The rotational symmetry is broken by the s-wave EI order parameter, and the anisotropic absorption together with possible lattice reconstruction can be used as signatures for this spin-triplet topological EI phase. Large amounts of spin-triplet excitons emerge spontaneously when an EI is achieved and exciton spin-Hall effect may be observed.

I. INTRODUCTION

Quantum spin-Hall insulators (QSHIs) have insulating bulk gaps and gapless edge states, which support nondissipative helical transport at the edges [1–6]. This is due to the nontrivial band topology they possess. In analogy to the superconductor, the excitonic insulator (EI) is another quantum state of matter which has received intensive research attention in recent years [7–16]. It was proposed by Keldysh and Kopaev, Kohn, and Jérome *et al.* in the 1960s [17–19], and consists of a phase in which bound excitons composed of electron-hole pairs form a condensate when the exciton binding energy E_b exceeds the band gap E_g. In EIs, a detectable quasiparticle gap-opening resembles the superconductors, but no charge transport exists [20]. This hinders their experimental detection by transport measurements. Over the last half-century, massive efforts have been made to realize EIs and much progress has been achieved. There have been several experimental indications for EIs in materials with lattice instability like $1T$-$TiSe_2$ [21,22] and Ta_2NiSe_5 [9–11], in artificial heterostructures like InAs/GaSb quantum well [7] and $MoSe_2$/WSe_2 bilayers [8], and in stable monolayer WTe_2 [23,24]. Nevertheless, it is fair to say that a systematic strategy to identify the EI phase is still absent.

From the theoretic point of view, the realization of the EI phase requires reduced screening of the Coulomb interactions, which is drastic in two-dimensional (2D) systems. However, 2D semiconductors with large E_b tend to have large E_g, as both of them are inversely proportional to the magnitude of screening [25]. To break this synergy, one strategy is to seek dipole-forbidden transitions near the band edges [12–14]. This may further lead us to find some nontrivial topological EIs (TEIs). The strategy is to find inversion-symmetric QSHIs whose band inversion does not happen between the conduction band minimum (CBM) and valence band maximum (VBM), but between a far-away band and the CBM+VBM. If the band inversion happens between the CBM and VBM, according to Fu-Kane criterion [26], the CBM and VBM must have opposite parity to make the Z_2 index nontrivial. But when the band inversion is between a far-away band and the CBM+VBM, the parity of CBM and VBM can be the same, as long as the far-away band has the opposite parity to them. Spin-orbital coupling (SOC) opens a gap between the CBM and VBM. In this way, the band-edge states possess the same parity so the dipole transitions are forbidden, and the EI phase may be achieved.

In this Letter, we demonstrate that these desired excitonic instabilities with topological features can exist in such QSHI materials like 2D arsenene oxide (AsO) and $Mo_2TiC_2O_2$ [27,28]. They are selected from published works about QSHIs following the aforementioned strategy, and they are stable according to the phonon calculations [27,28].
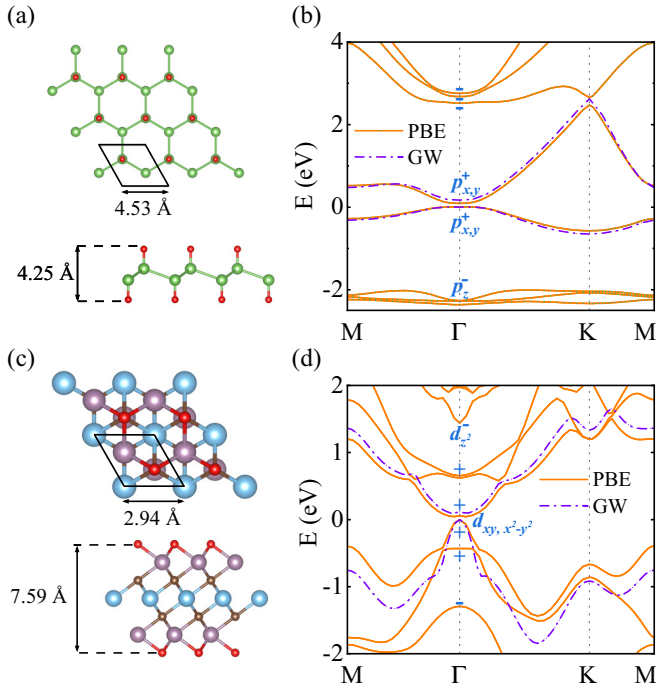
*ylshao@iphy.ac.cn
†xzli@pku.edu.cn

FIG. 1. (a), (c) Top and side (bottom) views of the atomic structures of (a) AsO and (c) $Mo_2TiC_2O_2$. Green, red, blue, purple, and brown balls denote the As, O, Ti, Mo, and C atoms, respectively. (b), (d) The PBE (orange solid lines) and *GW* (purple dot-dashes lines) band structures of (b) AsO and (d) $Mo_2TiC_2O_2$. The blue symbols mark the parity of the bands near the Fermi level.

First-principles *GW* approximation and Bathe-Salpeter equation (BSE) results show that the exciton binding energies (E_b) are larger than the *GW* band gaps (E_g), confirming the existence of the EI phase. Their low-energy physics can be described by the same model Eq. (1). Detailed analysis shows that the EI in this model is of spin-triplet type as a result of the nontrivial band geometry. The rotational symmetry is broken by the *s*-wave EI order parameter, and the anisotropic absorption together with possible lattice reconstruction can be used as signatures for this phase. Large amounts of spin-triplet excitons exist when EI is achieved and exciton spin-Hall effect may be detected by the deviations of the static spin Hall conductivity from the QSHI phase, which is also experimental evidence for the spin-triplet TEI phase. Considering the fact that not much effort has been made in realizing EIs in such topological materials [15,29–31], we believe that more TEIs can be found by a systematic search in real materials according to this strategy [32]. The coupling between EIs and topology demonstrated also means that rich physics can exist in materials retaining multiple features.

II. MATERIALS

Figures 1(a) and 1(c) show the lattice structure of 2D AsO and $Mo_2TiC_2O_2$, respectively. AsO has a structure similar to hexagonal 2D decorated stanene [28,33] and $Mo_2TiC_2O_2$ is a typical material of MXene family [27]. They both have C_3 rotational symmetry and inversion symmetry, and the band inversion happens at the Γ point between the p_z orbital with
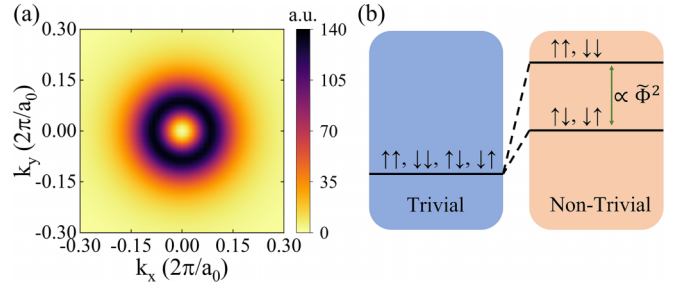

FIG. 2. (a) Berry curvature for spin-up sector calculated from the $k \cdot p$ model. (b) Schematics for the band geometric effects on the 1*s* exciton energy levels. Here $\tilde{\Phi}$ means the average value of $\tilde{\Phi}_k$ in the region where the 1*s* exciton wave-function extends.

negative parity and the $p_x \pm ip_y$ ones with positive parity in AsO, and between the d_{z^2} orbital with negative parity and the $d_{xy} \pm id_{x^2-y^2}$ ones with positive parity in $Mo_2TiC_2O_2$. p_z and d_{z^2} orbitals are far from the Fermi level, while $p_x \pm ip_y$ and $d_{xy} \pm id_{x^2-y^2}$ orbitals are near the Fermi level [Figs. 1(b) and 1(d)], where SOC contributes to open a band gap between them [27,28,34,35]. The *GW* band structure does not change significantly from the PBE one except that the band gap value increases from 93 meV to 165 meV in AsO, and from 57 meV to 115 meV in $Mo_2TiC_2O_2$ (the SOC was included in the DFT and *GW* calculations). After solving the BSE, we obtain large 1*s* exciton binding energies, $\sim$300 meV in AsO and $\sim$350 meV in $Mo_2TiC_2O_2$, as the band-edge states have the same parity [12]. These E_b values exceed the *GW* band gaps, indicating excitonic instability in these two materials.

III. MODEL

To explain the EI properties in more detail, we build the four-band low-energy $k \cdot p$ model near band edges at Γ point [36]. Including SOC, the Hamiltonian reads [36]

$$H_0(\boldsymbol{k}) = h_0(\boldsymbol{k})\tau_0 s_0 + \alpha(k_x^2 - k_y^2)\tau_x s_0 + 2\alpha k_x k_y \tau_y s_0 + \lambda \tau_z s_z,$$

$$= \begin{pmatrix} h_0(\boldsymbol{k}) + \lambda & 0 & \alpha k_-^2 & 0 \\ 0 & h_0(\boldsymbol{k}) - \lambda & 0 & \alpha k_-^2 \\ \alpha k_+^2 & 0 & h_0(\boldsymbol{k}) - \lambda & 0 \\ 0 & \alpha k_+^2 & 0 & h_0(\boldsymbol{k}) + \lambda \end{pmatrix}.$$

(1)

Here $h_0(\boldsymbol{k}) = \epsilon_0 + c(k_x^2 + k_y^2)$, $k_\pm = k_x \pm iky$, and λ is the SOC strength. τ_i and s_i ($i = 0, x, y, z$) are the Pauli matrices in the orbital space ($p_x \pm ip_y$ for AsO and $d_{xy} \pm id_{x^2-y^2}$ for $Mo_2TiC_2O_2$) and the up/down spin space. This Hamiltonian respects three-fold rotational symmetry $C_3 = \text{diag}(-1, e^{i\pi/3}, e^{-i\pi/3}, -1)$, inversion symmetry $I = \tau_0 s_0$ and time-reversal symmetry $\mathcal{T} = \tau_x s_y K$, where K is complex conjugation operator. The parameters ϵ_0, c, α and λ are fitted to reproduce the *GW* band structure near the Γ point. As H_0 is spin-diagonal, we can explicitly calculate the Chern number for both spin sectors by integrating the Berry curvature using $C_{\uparrow/\downarrow} = \frac{1}{2\pi} \iint \mathcal{F}_{\uparrow/\downarrow} dk_x dk_y$, and $\mathcal{F}_\uparrow$ is shown in Fig. 2(a). $C_{\uparrow/\downarrow} = \pm 1$ and the spin Chern number is $C_s = \frac{1}{2}(C_\uparrow - C_\downarrow) = 1$,

signaling non-trivial topology of the system, and in alignment with the analysis of the band structure.

On top of this single-particle picture, we further explore the excitonic properties. The model BSE based on the $k\cdot$ model reads [37]

$$(E_S - \epsilon_{n_c}(\boldsymbol{k}) + \epsilon_{n_v}(\boldsymbol{k}))A^S_{n_c n_v}(\boldsymbol{k}) = \sum_{n'_c, n'_v, \boldsymbol{k}'} \mathcal{K}_{n_c n_v \boldsymbol{k}, n'_c n'_v \boldsymbol{k}'} A^S_{n'_c, n'_v}(\boldsymbol{k}'), \tag{2}$$

where $n_c \in \{c\uparrow, c\downarrow\}$, $n_v \in \{v\uparrow, v\downarrow\}$, $\epsilon_{n_c}(\boldsymbol{k})$ [$\epsilon_{n_v}(\boldsymbol{k})$] is the quasiparticle energy of the conduction (valence) band, and $|S\rangle = \sum_{n_c n_v \boldsymbol{k}} A^S_{n_c n_v}(\boldsymbol{k})\hat{c}^\dagger_{n_c \boldsymbol{k}}\hat{c}_{n_v \boldsymbol{k}}|\text{GS}\rangle$ is the exciton eigenstate. The kernel reads [37,38] $\mathcal{K}_{n_c n_v \boldsymbol{k}, n'_c n'_v \boldsymbol{k}'} = -W(\boldsymbol{k} - \boldsymbol{k}')\Lambda_{n_c n'_c}(\boldsymbol{k}, \boldsymbol{k}')\Lambda_{n'_v n_v}(\boldsymbol{k}', \boldsymbol{k})/\Omega$, where Ω is the area and $W(\boldsymbol{q})$ is the screened Coulomb interaction, which equals $2\pi/[|q|(1 + 2\pi|q|\alpha_{2D})]$. α_{2D} is the 2D polarizability obtained from first-principles calculation. The form factors $\Lambda_{nn'}(\boldsymbol{k}, \boldsymbol{k}') = \langle n\boldsymbol{k}|n'\boldsymbol{k}'\rangle$ are calculated from the single-particle eigenvectors $|n\boldsymbol{k}\rangle$. Here we only include the direct part of the kernel, as the exchange part $\mathcal{K}^{\text{ex}}_{n_c n_v \boldsymbol{k}, n'_c n'_v \boldsymbol{k}'} = V(\boldsymbol{k} - \boldsymbol{k}')\Lambda_{n_c n_v}(\boldsymbol{k}, \boldsymbol{k})\Lambda_{n'_v n'_c}(\boldsymbol{k}', \boldsymbol{k}')/\Omega$ equals zero due to the orthogonality of the eigenstates [38]. As H_0 is spin diagonal, we can consider the like-spin ($c\uparrow v\uparrow$ and $c\downarrow v\downarrow$) and unlike-spin ($c\uparrow v\downarrow$ and $c\downarrow v\uparrow$) excitons separately [37]. Here we label the spin of a state in the electron picture to avoid misunderstanding [39] and choose the gauge by requiring that the lowest energy exciton state is in analogy of $1s$ state in the 2D hydrogen model [36,40,41]. The binding energies calculated from this model BSE match the first-principles results within 1 meV, implying that the key physics is captured in this model. Further, we find that the energies of the unlike-spin $1s$ excitons are lower than the like-spin $1s$ excitons, also in alignment with the first-principles results. This indicates that the EI phase is of the spin-triplet type.

IV. BAND GEOMETRY

Now we discuss the origin of the spin-triplet exciton ground state. We define $U_{ij}(\boldsymbol{k}, \boldsymbol{k}') \equiv W(\boldsymbol{k} - \boldsymbol{k}')\Lambda_{ii}(\boldsymbol{k}, \boldsymbol{k}')\Lambda_{jj}(\boldsymbol{k}', \boldsymbol{k})$ as an effective interaction, where $i, j \in \{c\uparrow, c\downarrow, v\uparrow, v\downarrow\}$. It is smaller than the $W(\boldsymbol{k} - \boldsymbol{k}')$ as a result of the Bloch form factors. As H_0 is isotropic, we can decompose these quantities into different angular momentum channels, and find that [36,40]

$$U^{1s}_{c\uparrow v\downarrow}(\boldsymbol{k}, \boldsymbol{k}') = U^{1s}_{c\downarrow v\uparrow}(\boldsymbol{k}, \boldsymbol{k}'), U^{1s}_{c\uparrow v\uparrow}(\boldsymbol{k}, \boldsymbol{k}') = U^{1s}_{c\downarrow v\downarrow}(\boldsymbol{k}, \boldsymbol{k}'),$$

$$U^{1s}_{c\uparrow v\downarrow}(\boldsymbol{k}, \boldsymbol{k}') - U^{1s}_{c\uparrow v\uparrow}(\boldsymbol{k}, \boldsymbol{k}') = [W^0(k, k') - W^4(k, k')]\tilde{\Phi}_k\tilde{\Phi}_{k'}, \tag{3}$$

where $W(\boldsymbol{k}_1 - \boldsymbol{k}_2) = \sum_m W^m(k_1, k_2)e^{im(\theta_1 - \theta_2)}$, $\tilde{\Phi}_k = \Phi_k/4\pi \in (0, 1/2)$, and Φ_k is the spin-up valence band's Berry curvature flux through the circle around Γ with radius k. As a result of the long-range nature of the screened Coulomb interaction, $W^0(k, k') > W^4(k, k')$, we can conclude that the effective interaction in the $1s$ unlike-spin channel is larger than that in the like-spin channel. For trivial bands with zero Berry curvature flux, the like- and unlike-spin $1s$ excitons are degenerate. Therefore, it can be clearly seen that the spin-triplet nature of the lowest energy exciton state is linked to H_0's nontrivial band geometry [40,42], which is shown schematically in Fig. 2(b).

V. TEI PHASE

To investigate the EI phase in more detail, we performed Hartree-Fock calculations at 0 K based on the $k \cdot p$ model [36]. The Hartree-Fock mean-field Hamiltonian in the eigenbasis reads $\hat{H}_{\text{MF}} = \sum_{\boldsymbol{k}} \Psi^\dagger_{\boldsymbol{k}}(H_{\text{eig}} + H_{\text{Fock}})\Psi_{\boldsymbol{k}}$, where $H_{\text{eig}}(\boldsymbol{k}) = \text{diag}(\epsilon_{c\uparrow}(\boldsymbol{k}), \epsilon_{c\downarrow}(\boldsymbol{k}), \epsilon_{v\uparrow}(\boldsymbol{k}), \epsilon_{v\downarrow}(\boldsymbol{k}))$ and

$$H_{\text{Fock}}(\boldsymbol{k}) = \begin{pmatrix} \Delta_{c\uparrow c\uparrow}(\boldsymbol{k}) & \Delta_{c\uparrow c\downarrow}(\boldsymbol{k}) & \Delta_{c\uparrow v\uparrow}(\boldsymbol{k}) & \Delta_{c\uparrow v\downarrow}(\boldsymbol{k}) \\ \Delta^*_{c\uparrow c\downarrow}(\boldsymbol{k}) & \Delta_{c\downarrow c\downarrow}(\boldsymbol{k}) & \Delta_{c\downarrow v\uparrow}(\boldsymbol{k}) & \Delta_{c\downarrow v\downarrow}(\boldsymbol{k}) \\ \Delta^*_{c\uparrow v\uparrow}(\boldsymbol{k}) & \Delta^*_{c\downarrow v\uparrow}(\boldsymbol{k}) & \Delta_{v\uparrow v\uparrow}(\boldsymbol{k}) & \Delta_{v\uparrow v\downarrow}(\boldsymbol{k}) \\ \Delta^*_{c\uparrow v\downarrow}(\boldsymbol{k}) & \Delta^*_{c\downarrow v\downarrow}(\boldsymbol{k}) & \Delta^*_{v\uparrow v\downarrow}(\boldsymbol{k}) & \Delta_{v\downarrow v\downarrow}(\boldsymbol{k}) \end{pmatrix}, \tag{4}$$

$$\Delta_{ij}(\boldsymbol{k}) = -\frac{1}{\Omega}\sum_{\boldsymbol{k}'} U_{ij}(\boldsymbol{k}, \boldsymbol{k}')\rho_{ij}(\boldsymbol{k}'). \tag{5}$$

The density matrix $\rho_{ij}(\boldsymbol{k}) = \langle c^\dagger_{j\boldsymbol{k}}c_{i\boldsymbol{k}}\rangle - \delta_{ij}\delta_{i=vs}$ is defined relative to the fully filled valence band to avoid the double counting of the interaction and

$$\langle c^\dagger_{j\boldsymbol{k}}c_{i\boldsymbol{k}}\rangle = \sum_\alpha [\mathcal{U}]_{i,\alpha} f_{\text{F}}(E_{\boldsymbol{k},\alpha})[\mathcal{U}^\dagger]_{\alpha,j}. \tag{6}$$

$\mathcal{U}$ is the unitary matrix that diagonalizes the $\hat{H}_{\text{MF}}$, $E_{\boldsymbol{k},i}$s are the corresponding eigenvalues, and f_{F} is the Fermi-Dirac distribution function. The Hartree energy reads $E_{\text{Hartree}} = \frac{1}{2\Omega^2}\sum_{ij,\boldsymbol{k}_1\boldsymbol{k}_2} W(0)\rho_{ii}(\boldsymbol{k}_1)\rho_{jj}(\boldsymbol{k}_2)$, which vanishes as $\sum_i \rho_{ii}(\boldsymbol{k}) = 0$. We choose different initial Δ_{ij}s, or, equivalently, ρ_{ij}s, and solve the Hartree-Fock equations above in a dense k-point mesh by iterations. Then the total energy density can be calculated by $E_{\text{total}} = \frac{1}{2\Omega}\sum_{\boldsymbol{k}} \text{Tr}\{\rho(\boldsymbol{k})[H_{\text{eig}}(\boldsymbol{k}) + H_{\text{MF}}(\boldsymbol{k})]\}$, and we compare the energies to determine the ground state. On realistic substrates, screening can be estimated by substituting $W(q)$ with $W'(q) = 2\pi/[q(\epsilon + 2\pi q\alpha_{2D})]$, where $\epsilon = (1 + \epsilon_{\text{r}})/2$ (ϵ_{r} is the dielectric constant of the substrate). In Fig. 3(a), we show the Hartree-Fock phase diagram with respect to ϵ_{r}.

When ϵ_{r} is small, the $1s$ exciton binding energy is much larger than the band gap. Among the excitonic order parameters $\Delta_{cv}(\boldsymbol{k})$s, only the unlike-spin ones $\Delta_{c\uparrow v\downarrow}(\boldsymbol{k})$, $\Delta_{c\downarrow v\uparrow}(\boldsymbol{k})$ are nonzero [(Fig. 3(b)] due to the band geometric effects explained before, and the band structures in this EI phase are different from the original ones [see the lower insets of Fig. 3(a)]. A prominent increase of the band gap emerges, the conduction band flattens, and the valence band distort strongly, making the gap more indirect than before. The rotational symmetry is broken by the s-wave excitonic order parameters, while time-reversal symmetry and inversion symmetry are preserved, and the bands are still twofold degenerate everywhere in the k space due to the Kramers' theorem. To identify the topological property, we calculate the Wilson loop for the two degenerate occupied bands [43,44]. The 2×2 overlap matrix $F^{n,n+1}_{i,j} = \langle i^n \mid j^{n+1}\rangle$ along square loops around Γ (n is the step index in the loop), where $i, j \in \{v\uparrow, v\downarrow\}$, are calculated [31]. The phase angles θ_k correspond to the eigenvalues $e^{i\theta_k}$ of the product of all Fs in one loop labeled by $|k|$, where $|k|$ is half of the square's side length. As shown in Fig. 4(a), each occupied band winds the cylinder once in
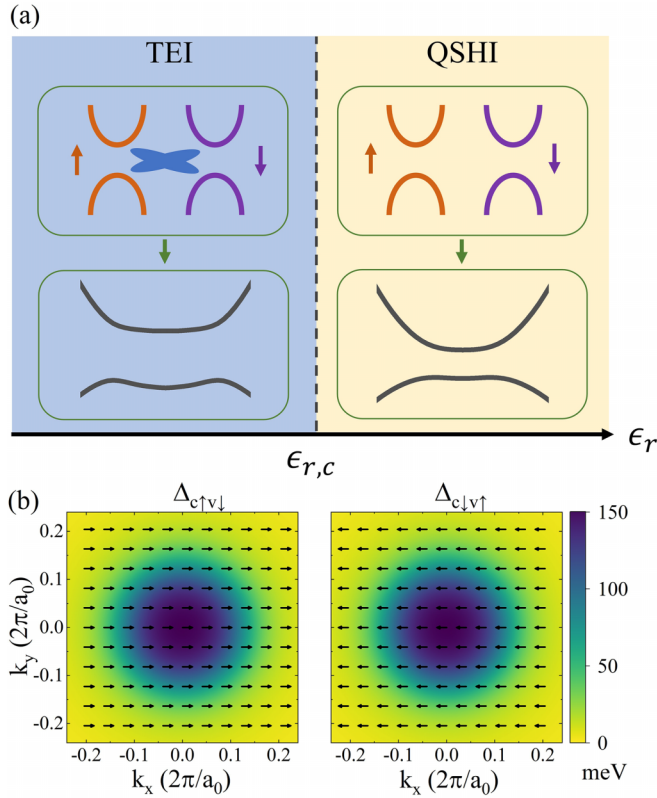
FIG. 3. (a) The excitonic mean-field phase diagram with respect to different substrate dielectric constants. TEI and QSHI represent the topological EI phase and normal quantum spin-Hall insulator phase, respectively. The upper insets show the excitonic pairing channels in these phases schematically, and the lower insets show the band structures in these phases. $\epsilon_{r,c}$ refer to the phase-transition points. (b) The absolute values and phase winding patterns of the nonzero excitonic order parameters at 0 K in the reciprocal space. The direction of the arrow denotes the phase angle and the color map indicates the magnitude.

opposite directions, indicating that the nontrivial Z_2 topology survives in the excitonic phase, and we label it TEI.

When ϵ_r further increases and exceeds a critical value $\epsilon_{r,c}$ where the exciton binding energy equals the band gap, the excitonic order parameters are all zero and the EI phase disappears. Now the system is the normal QSHI. Numerical results show that $\epsilon_{r,c} = 6.7$ for AsO and $\epsilon_{r,c} = 9.6$ for Mo$_2$TiC$_2$O$_2$, indicating that the TEI phase is achievable on realistic substrates in experiments.

VI. EXPERIMENTS

Symmetry breaking can be used to detect the EI phase experimentally. For example, a charge-density wave emerges in WTe$_2$ [23,24] as the excitons condensate at finite momentum, breaking the translational symmetry. As for the TEI phase here, the broken symmetry is the C_3 rotational symmetry, which is a result of the s-wave excitonic order parameters [Fig. 3(a)]. The C_3 breaking of the electronic system may affect the lattice symmetry by the electron-phonon coupling, which can be probed by experiments such as XRD and STM.
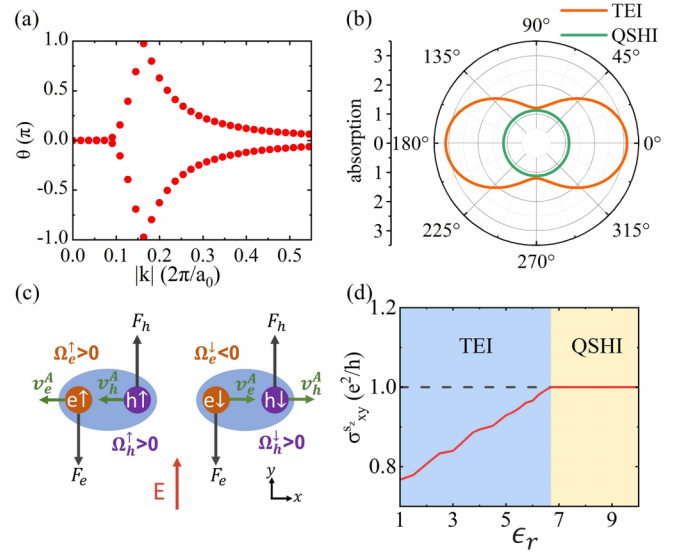

FIG. 4. (a) Results of Wilson-loop calculation for the TEI phase, where the red dots represent the phase angles of the two occupied bands. (b) Absorption intensity at $\omega = 0.4$ eV with different polarization directions. (c) A schematic diagram for the exciton spin-Hall effect. The electron and hole for each spin-triplet exciton will obtain an anomalous velocity $\boldsymbol{v}_{e/h}^{A} = -\dot{\mathbf{k}}_{e/h} \times \boldsymbol{\Omega}_{e/h}$ pointing in the same direction. (d) Static spin Hall conductivity with respect to different ϵ_rs. (b) and (d) are calculated at 0 K using AsO parameters.

Besides, as shown in Fig. 4(b), the absorption spectrum will be anisotropic as well, which can be demonstrated by the real part of the optical conductivity:

$$\sigma_a(\omega) = \frac{1}{\Omega} \sum_{m \in c, n \in v} \sum_{\mathbf{k}} \frac{4ie^2\omega \mathcal{O}_{\mathbf{k},nm}^a (f_{\mathrm{F}}(E_{\mathbf{k},n}) - f_{\mathrm{F}}(E_{\mathbf{k},m}))}{\hbar\omega + i\eta + E_{\mathbf{k},n} - E_{\mathbf{k},m}},$$
(7)

$$\mathcal{O}_{\mathbf{k},nm}^a = \frac{\hbar^2 |\hat{v}_{nm}^a(\mathbf{k})|^2}{(E_{\mathbf{k},n} - E_{\mathbf{k},m})^2}.$$
(8)

Here a labels the direction of the polarization and the vertex correction can be safely neglected as the collective modes are dark due to the same-parity band edge states [45–49].

Large amounts of spin-triplet excitons emerge spontaneously when TEI is achieved. For the $c \uparrow v \downarrow$ ($c \downarrow v \uparrow$) exciton, or the $e \uparrow h \uparrow$ ($e \downarrow h \downarrow$) exciton equivalently, the electron and hole have Berry curvature with opposite signs ($\Omega_e^\uparrow$, $\Omega_h^\downarrow < 0$ and $\Omega_e^\downarrow$, $\Omega_h^\uparrow > 0$). From the semiclassical equations of motion for the exciton $\dot{\mathbf{K}} = \dot{\mathbf{k}}_e + \dot{\mathbf{k}}_h = 0$, $\dot{\mathbf{R}} = (\partial_{\mathbf{k}_e}\varepsilon_{\mathbf{k}_e}^e + \partial_{\mathbf{k}_h}\varepsilon_{\mathbf{k}_h}^h)/2 - \dot{\mathbf{k}}_e \times (\boldsymbol{\Omega}_e - \boldsymbol{\Omega}_h)/2$, we can see that the spin-triplet exciton acquires a velocity in the transverse direction [50]. This will result in a net transverse spin transport as schematically shown in Fig. 4(c), and can be called the exciton spin-Hall effect. The static spin Hall conductivity can be calculated using [51,52]

$$\sigma_{xy}^{s_z} = \frac{1}{\Omega} \sum_{mn, m \neq n} \sum_{\mathbf{k}} \frac{-2\hbar e f_{\mathrm{F}}(E_{\mathbf{k},n}) \, \mathrm{Im}\left[\hat{j}_{x,nm}^{s_z}(\mathbf{k}) \hat{v}_{mn}^y(\mathbf{k})\right]}{(E_{\mathbf{k},n} - E_{\mathbf{k},m})^2},$$
(9)

where $\hat{j}_x^{s_z}$ is the spin current operator. In QSHI phase, $\sigma_{xy}^{s_z}$ equals $\frac{e^2}{h}$, and the spin Hall current is in the $+x$ direction

when the electric field is applied in the $+y$ direction. In the TEI phase, the spin Hall current of the spin-triplet excitons is in the $-x$ direction, as shown in Fig. 4(c). Therefore, the static spin Hall conductivity in the TEI phase is reduced from $\frac{e^2}{h}$ in the QSHI phase, as illustrated in Fig. 4(d). This can also be used as an experimental signature for the TEI phase.

The mean-field theory generally overestimates the exciton superfluid transition temperature due to the lack of quantum fluctuations. Instead, it should be estimated by the Berezinsky–Kosterlitz–Thouless (BKT) temperature [36,53,54], and we find that $T_{\mathrm{BKT}} \approx 27$ K for AsO and $T_{\mathrm{BKT}} \approx 65$ K for $Mo_2TiC_2O_2$, respectively, on hBN substrate where $\epsilon_{\mathrm{r}} \approx 5$. However, in real materials the hybridization between the conduction and valence bands is unavoidable, which breaks the electron (hole) U(1) symmetry [55]. The EI transition now only corresponds to the breaking of discrete symmetries (C_3 here), and a true exciton superfluid can never happen, where the collective mode will have a finite gap [46,47,55,56].

This TEI phase may have applications in different electronic, spintronic, and photonic devices. For example, there are exotic transport properties in the EI-based hybrid junction [57–59]. The topological edge states may also play an essential role in the transport [60] and optical [61] properties in the TEI phase, which deserve further investigation. We hope this combined use of QSHIs with EI may stimulate more theoretical and experimental studies in such interdisciplinary areas.

Note added. Recently, we became aware of Ref. [62], whose results are consistent with ours in the finite overlapping part.

ACKNOWLEDGMENTS

[1] C. L. Kane and E. J. Mele, Quantum spin Hall effect in graphene, Phys. Rev. Lett. **95**, 226801 (2005).

[2] C. L. Kane and E. J. Mele, Z_2 topological order and the quantum spin Hall effect, Phys. Rev. Lett. **95**, 146802 (2005).

[3] C. Liu, T. L. Hughes, X.-L. Qi, K. Wang, and S.-C. Zhang, Quantum spin Hall effect in inverted type-II semiconductors, Phys. Rev. Lett. **100**, 236601 (2008).

[4] B. A. Bernevig, T. L. Hughes, and S.-C. Zhang, Quantum spin Hall effect and topological phase transition in HgTe quantum wells, Science **314**, 1757 (2006).

[5] L. Kou, Y. Ma, Z. Sun, T. Heine, and C. Chen, Two-dimensional topological insulators: Progress and prospects, J. Phys. Chem. Lett. **8**, 1905 (2017).

[6] M. S. Lodge, S. A. Yang, S. Mukherjee, and B. Weber, Atomically thin quantum spin Hall insulators, Adv. Mater. **33**, 2008029 (2021).

[7] L. Du, X. Li, W. Lou, G. Sullivan, K. Chang, J. Kono, and R.-R. Du, Evidence for a topological excitonic insulator in InAs/GaSb bilayers, Nat. Commun. **8**, 1971 (2017).

[8] Z. Wang, D. A. Rhodes, K. Watanabe, T. Taniguchi, J. C. Hone, J. Shan, and K. F. Mak, Evidence of high-temperature exciton condensation in two-dimensional atomic double layers, Nature (London) **574**, 76 (2019).

[9] Y. Wakisaka, T. Sudayama, K. Takubo, T. Mizokawa, M. Arita, H. Namatame, M. Taniguchi, N. Katayama, M. Nohara, and H. Takagi, Excitonic insulator state in Ta_2NiSe_5 probed by photoemission spectroscopy, Phys. Rev. Lett. **103**, 026402 (2009).

[10] Y. F. Lu, H. Kono, T. I. Larkin, A. W. Rost, T. Takayama, A. V. Boris, B. Keimer, and H. Takagi, Zero-gap semiconductor to excitonic insulator transition in Ta_2NiSe_5, Nat. Commun. **8**, 14408 (2017).

[11] S. Mor, M. Herzog, D. Golež, P. Werner, M. Eckstein, N. Katayama, M. Nohara, H. Takagi, T. Mizokawa, C. Monney, and J. Stähler, Ultrafast electronic band gap control in an excitonic insulator, Phys. Rev. Lett. **119**, 086401 (2017).

[12] Z. Jiang, Y. Li, S. Zhang, and W. Duan, Realizing an intrinsic excitonic insulator by decoupling exciton binding energy from the minimum band gap, Phys. Rev. B **98**, 081408(R) (2018).

[13] Z. Jiang, Y. Li, W. Duan, and S. Zhang, Half-excitonic insulator: A single-spin Bose-Einstein condensate, Phys. Rev. Lett. **122**, 236402 (2019).

[14] Z. Jiang, W. Lou, Y. Liu, Y. Li, H. Song, K. Chang, W. Duan, and S. Zhang, Spin-triplet excitonic insulator: The case of semihydrogenated graphene, Phys. Rev. Lett. **124**, 166401 (2020).

[15] D. Varsano, M. Palummo, E. Molinari, and M. Rontani, A monolayer transition-metal dichalcogenide as a topological excitonic insulator, Nat. Nanotechnol. **15**, 367 (2020).

[16] H. Yang, X. Wang, and X.-Z. Li, A scenario for high-temperature excitonic insulators, New J. Phys. **24**, 083010 (2022).

[17] L. V. Keldysh and Y. V. Kopaev, Possible instability of the semimetallic state toward Coulomb interaction, *Selected Papers of Leonid V Keldysh* (World Scientific, 2024), pp. 41–46.

[18] W. Kohn, Excitonic phases, Phys. Rev. Lett. **19**, 439 (1967).

[19] D. Jérome, T. M. Rice, and W. Kohn, Excitonic insulator, Phys. Rev. **158**, 462 (1967).

[20] B. I. Halperin and T. M. Rice, Possible anomalies at a semimetal-semiconductor transition, Rev. Mod. Phys. **40**, 755 (1968).

[21] H. Cercellier, C. Monney, F. Clerc, C. Battaglia, L. Despont, M. G. Garnier, H. Beck, P. Aebi, L. Patthey, H. Berger, and L. Forró, Evidence for an excitonic insulator phase in $1T-TiSe_2$, Phys. Rev. Lett. **99**, 146403 (2007).

[22] A. Kogar, M. S. Rak, S. Vig, A. A. Husain, F. Flicker, Y. I. Joe, L. Venema, G. J. MacDougall, T. C. Chiang, E. Fradkin, J. van

Wezel, and P. Abbamonte, Signatures of exciton condensation in a transition metal dichalcogenide, Science **358**, 1314 (2017).

[23] B. Sun, W. Zhao, T. Palomaki, Z. Fei, E. Runburg, P. Malinowski, X. Huang, J. Cenker, Y.-T. Cui, J.-H. Chu, X. Xu, S. S. Ataei, D. Varsano, M. Palummo, E. Molinari, M. Rontani, and D. H. Cobden, Evidence for equilibrium exciton condensation in monolayer WTe₂, Nat. Phys. **18**, 94 (2022).

[24] Y. Jia, P. Wang, C.-L. Chiu, Z. Song, G. Yu, B. Jäck, S. Lei, S. Klemenz, F. A. Cevallos, M. Onyszczak, N. Fishchenko, X. Liu, G. Farahi, F. Xie, Y. Xu, K. Watanabe, T. Taniguchi, B. A. Bernevig, R. J. Cava, L. M. Schoop *et al.*, Evidence for a monolayer excitonic insulator, Nat. Phys. **18**, 87 (2022).

[25] Z. Jiang, Z. Liu, Y. Li, and W. Duan, Scaling universality between band gap and exciton binding energy of two-dimensional semiconductors, Phys. Rev. Lett. **118**, 266401 (2017).

[26] L. Fu and C. L. Kane, Topological insulators with inversion symmetry, Phys. Rev. B **76**, 045302 (2007).

[27] C. Si, K.-H. Jin, J. Zhou, Z. Sun, and F. Liu, Large-gap quantum spin Hall state in MXenes: *d*-band topological order in a triangular lattice, Nano Lett. **16**, 6584 (2016).

[28] Y. Wang, W. Ji, C. Zhang, P. Li, S. Zhang, P. Wang, S. Li, and S. Yan, Two-dimensional arsenene oxide: A realistic large-gap quantum spin Hall insulator, Appl. Phys. Lett. **110**, 213101 (2017).

[29] J. C. Budich, B. Trauzettel, and P. Michetti, Time reversal symmetric topological exciton condensate in bilayer HgTe quantum wells, Phys. Rev. Lett. **112**, 146405 (2014).

[30] D. I. Pikulin and T. Hyart, Interplay of exciton condensation and the quantum spin Hall effect in InAs/GaSb bilayers, Phys. Rev. Lett. **112**, 176403 (2014).

[31] F. Xue and A. H. MacDonald, Time-reversal symmetry-breaking nematic insulators near quantum spin Hall phase transitions, Phys. Rev. Lett. **120**, 186802 (2018).

[32] In the experimentally confirmed topological EI WTe₂, the conduction band minimum and valence band maximum are located at different *k* points and the possible excitonic instability will then break translational symmetry and generate charge density waves, which is very different with the systems discussed here [23,24].

[33] Y. Xu, B. Yan, H.-J. Zhang, J. Wang, G. Xu, P. Tang, W. Duan, and S.-C. Zhang, Large-gap quantum spin Hall insulators in tin films, Phys. Rev. Lett. **111**, 136804 (2013).

[34] J. Deng, D. Shao, J. Gao, C. Yue, H. Weng, Z. Fang, and Z. Wang, Twisted nodal wires and three-dimensional quantum spin Hall effect in distorted square-net compounds, Phys. Rev. B **105**, 224103 (2022).

[35] Using the language of topological quantum chemistry [65], the number of elementary band representations near the Fermi level in the absence (presence) of SOC is one in AsO, and can be labeled as (1, 1) in the convention of Ref. [34]. For Mo₂TiC₂O₂, the number of elementary band representations near the Fermi level in the absence (presence) of SOC is 2(2), and can be labeled as (2, 2).

[36] See Supplemental Material at http://link.aps.org/supplemental/10.1103/PhysRevB.109.075167 for the details of first-principles calculations, derivation for the $k \cdot p$ models and gauge choice, exciton optical selection rules, details of the band geometry analysis on exciton energies, details of the Hartree-Fock calculations, and discussions of the superfluidity, which also includes Refs. [66–74].

[37] M. Rohlfing and S. G. Louie, Electron-hole excitations and optical spectra from first principles, Phys. Rev. B **62**, 4927 (2000).

[38] B. Scharf, G. Xu, A. Matos-Abiague, and I. Žutić, Magnetic proximity effects in transition-metal dichalcogenides: Converting excitons, Phys. Rev. Lett. **119**, 127403 (2017).

[39] For example, a $c \uparrow v \downarrow$ exciton consists of a spin-up occupied state in thr conduction band and a spin-down unoccupied state in the valence band. Equivalently speaking, it consists of a spin-up electron and a spin-up hole ($e \uparrow h \uparrow$), which is a spin-triplet exciton.

[40] J. Zhou, W.-Y. Shan, W. Yao, and D. Xiao, Berry phase modification to the energy spectrum of excitons, Phys. Rev. Lett. **115**, 166803 (2015).

[41] X. Zhang, W.-Y. Shan, and D. Xiao, Optical selection rule of excitons in gapped chiral fermion systems, Phys. Rev. Lett. **120**, 077401 (2018).

[42] A. Srivastava and A. Imamoğlu, Signatures of Bloch-band geometry on excitons: Nonhydrogenic spectra in transition-metal dichalcogenides, Phys. Rev. Lett. **115**, 166802 (2015).

[43] R. Yu, X. L. Qi, A. Bernevig, Z. Fang, and X. Dai, Equivalent expression of Z₂ topological invariant for band insulators using the non-Abelian Berry connection, Phys. Rev. B **84**, 075119 (2011).

[44] H. Weng, R. Yu, X. Hu, X. Dai, and Z. Fang, Quantum anomalous Hall effect and related topological electronic states, Adv. Phys. **64**, 227 (2015).

[45] Z. Khatibi, R. Ahemeh, and M. Kargarian, Excitonic insulator phase and condensate dynamics in a topological one-dimensional model, Phys. Rev. B **102**, 245121 (2020).

[46] Y. Murakami, D. Golež, T. Kaneko, A. Koga, A. J. Millis, and P. Werner, Collective modes in excitonic insulators: Effects of electron-phonon coupling and signatures in the optical response, Phys. Rev. B **101**, 195118 (2020).

[47] D. Golež, Z. Sun, Y. Murakami, A. Georges, and A. J. Millis, Nonlinear spectroscopy of collective modes in an excitonic insulator, Phys. Rev. Lett. **125**, 257601 (2020).

[48] T. Tanabe, T. Kaneko, and Y. Ohta, Third-harmonic generation in excitonic insulators, Phys. Rev. B **104**, 245103 (2021).

[49] T. Kaneko, Z. Sun, Y. Murakami, D. Golež, and A. J. Millis, Bulk photovoltaic effect driven by collective excitations in a correlated insulator, Phys. Rev. Lett. **127**, 127402 (2021).

[50] S. Chaudhary, C. Knapp, and G. Refael, Anomalous exciton transport in response to a uniform in-plane electric field, Phys. Rev. B **103**, 165119 (2021).

[51] J. Sinova, S. O. Valenzuela, J. Wunderlich, C. H. Back, and T. Jungwirth, Spin Hall effects, Rev. Mod. Phys. **87**, 1213 (2015).

[52] Y. Yao and Z. Fang, Sign changes of intrinsic spin Hall effect in semiconductors and simple metals: First-principles calculations, Phys. Rev. Lett. **95**, 156601 (2005).

[53] V. Berezinskii, Destruction of long-range order in one-dimensional and two-dimensional systems having a continuous symmetry group I. Classical systems, Sov. Phys. JETP **32**, 493 (1971).

[54] J. M. Kosterlitz and D. J. Thouless, Ordering, metastability and phase transitions in two-dimensional systems, J. Phys. C: Solid State Phys. **6**, 1181 (1973).

[55] G. Mazza, M. Rösner, L. Windgätter, S. Latini, H. Hübener, A. J. Millis, A. Rubio, and A. Georges, Nature of symmetry

breaking at the excitonic insulator transition: Ta_2NiSe_5, Phys. Rev. Lett. **124**, 197601 (2020).

[56] Z. Sun, T. Kaneko, D. Golež, and A. J. Millis, Second-order Josephson effect in excitonic insulators, Phys. Rev. Lett. **127**, 127702 (2021).

[57] M. Rontani and L. J. Sham, Coherent transport in a homojunction between an excitonic insulator and semimetal, Phys. Rev. Lett. **94**, 186404 (2005).

[58] D. Bercioux, T. M. Klapwijk, and F. S. Bergeret, Transport properties of an electron-hole bilayer in contact with a superconductor hybrid junction, Phys. Rev. Lett. **119**, 067001 (2017).

[59] D. Bercioux, B. Bujnowski, and F. S. Bergeret, Quantum transport properties of an exciton insulator/superconductor hybrid junction, Adv. Quantum Technol. **2**, 1800049 (2019).

[60] K. Ziegler, A. Sinner, and Y. E. Lozovik, Anomalous Josephson effect of s-wave pairing states in chiral double layers, Phys. Rev. Lett. **128**, 157001 (2022).

[61] B. Hou, D. Wang, B. A. Barker, and D. Y. Qiu, Exchange-driven intermixing of bulk and topological surface states by chiral excitons in Bi_2Se_3, Phys. Rev. Lett. **130**, 216402 (2023).

[62] S. Dong and Y. Li, Robust high-temperature topological excitonic insulator of transition-metal carbide MXenes, Phys. Rev. B **107**, 235147 (2023).

[63] P. Giannozzi, S. Baroni, N. Bonini, M. Calandra, R. Car, C. Cavazzoni, D. Ceresoli, G. L. Chiarotti, M. Cococcioni, I. Dabo, A. Dal Corso, S. de Gironcoli, S. Fabris, G. Fratesi, R. Gebauer, U. Gerstmann, C. Gougoussis, A. Kokalj, M. Lazzeri, L. Martin-Samos *et al.*, QUANTUM ESPRESSO: A modular and open-source software project for quantum simulations of materials, J. Phys.: Condens. Matter **21**, 395502 (2009).

[64] D. Sangalli, A. Ferretti, H. Miranda, C. Attaccalite, I. Marri, E. Cannuccia, P. Melo, M. Marsili, F. Paleari, A. Marrazzo, G. Prandini, P. Bonfà, M. O. Atambo, F. Affinito, M. Palummo, A. Molina-Sánchez, C. Hogan, M. Grüning, D. Varsano, and A. Marini, Many-body perturbation theory calculations using the yambo code, J. Phys.: Condens. Matter **31**, 325902 (2019).

[65] B. Bradlyn, L. Elcoro, J. Cano, M. G. Vergniory, Z. Wang, C. Felser, M. I. Aroyo, and B. A. Bernevig, Topological quantum chemistry, Nature (London) **547**, 298 (2017).

[66] J. P. Perdew, K. Burke, and M. Ernzerhof, Generalized gradient approximation made simple, Phys. Rev. Lett. **77**, 3865 (1996).

[67] D. R. Hamann, Optimized norm-conserving Vanderbilt pseudopotentials, Phys. Rev. B **88**, 085117 (2013).

[68] P. Scherpelz, M. Govoni, I. Hamada, and G. Galli, Implementation and validation of fully relativistic GW calculations: Spin–orbit coupling in molecules, nanocrystals, and solids, J. Chem. Theory Comput. **12**, 3523 (2016).

[69] S. Konschuh, M. Gmitra, and J. Fabian, Tight-binding theory of the spin-orbit coupling in graphene, Phys. Rev. B **82**, 245412 (2010).

[70] G. Sethi, M. Cuma, and F. Liu, Excitonic condensate in flat valence and conduction bands of opposite chirality, Phys. Rev. Lett. **130**, 186401 (2023).

[71] L. Reining, The GW approximation: Content, successes and limitations, WIREs Computat. Mol. Sci. **8**, e1344 (2018).

[72] S. Peotta and P. Törmä, Superfluidity in topologically nontrivial flat bands, Nat. Commun. **6**, 8944 (2015).

[73] L. Liang, T. I. Vanhala, S. Peotta, T. Siro, A. Harju, and P. Törmä, Band geometry, Berry curvature, and superfluid weight, Phys. Rev. B **95**, 024515 (2017).

[74] X. Hu, T. Hyart, D. I. Pikulin, and E. Rossi, Quantum-metric-enabled exciton condensate in double twisted bilayer graphene, Phys. Rev. B **105**, L140506 (2022).